

# Graphene Nanomeshes: Existence of Defect-Induced Dirac Fermions on Graphene Host Matrix

H. Şahin<sup>1</sup> and S. Ciraci<sup>1,2,\*</sup>

<sup>1</sup>*UNAM-Institute of Materials Science and Nanotechnology, Bilkent University, 06800 Ankara, Turkey*

<sup>2</sup>*Department of Physics, Bilkent University, 06800 Ankara, Turkey*

(Dated: April 18, 2022)

Motivated by the state of the art method for fabricating high density periodic nanoscale defects in graphene, the structural, mechanical and electronic properties of defect-patterned graphene nanomeshes including diverse morphologies of adatoms and holes are investigated by means of first-principles calculations within density functional theory. It is found that various patterns of adatom groups yield metallic or semimetallic, even semiconducting behavior and specific patterns can be in a magnetic state. Even though the patterns of single adatoms dramatically alter the electronic structure of graphene, adatom groups of specific symmetry can maintain the Dirac fermion behavior. Nanoholes forming nanomesh are also investigated. Depending on the interplay between the repeat periodicity and the geometry of the hole, the nanomesh can be in different states ranging from metallic to semiconducting including semimetallic state with the bands crossing linearly at the Fermi level. We showed that forming periodically repeating superstructures in graphene matrix can develop a promising technique to engineer nanomaterials with desired electronic and magnetic properties.

PACS numbers: 81.05.ue, 73.22.Pr, 63.22.Rc, 61.48.Gh

## I. INTRODUCTION

Propagation of electron waves through the honeycomb lattice attributes exceptional features to graphene.<sup>1</sup> Conduction of electrons within one-atom-thick layer with minute scattering makes the observation of quantum effects possible even at room temperature.<sup>2,3</sup> Experimental investigations have reported the observation of half-integer quantum Hall effect for carriers in graphene and possible magneto-electronic device applications.<sup>4</sup> Most of the unique properties of graphene are related to its monolayer lattice structure, linearly crossed  $\pi$  bands at Fermi level with electron-hole symmetry. Recently, we showed that the honeycomb structure with linear band crossings at Dirac points is also common to Si and Ge.<sup>5,6</sup>

In an effort to make semimetallic graphene suitable for electronic applications, it has been functionalized to generate band gaps. It was theoretically shown that it is possible to induce band-gap opening produced by the adsorption of atomic hydrogen on graphene by choosing specific adsorption periodicity.<sup>7</sup> It was also experimentally shown that B- and N-doped graphenes can be synthesized to exhibit p- and n-type semiconducting properties that can be systematically tuned with the dopant concentration.<sup>8</sup> Effect of hydrogenation and the transition metal atom adsorption on the transport properties of graphene was also investigated theoretically.<sup>9,10</sup> Using symmetry arguments and tight binding calculations it was shown that the periodic structure of defects (such as B and N impurities) on graphene can exhibit semimetallic and semiconductor behavior.<sup>11</sup> Moreover, weak perturbation potential forming a large hexagonal lattice in a two dimensional electron gas was shown to lead a massless Dirac fermion Hamiltonian with linearly crossing bands at Dirac points.<sup>12-14</sup>

A majority of the current studies on graphene is devoted to its chemical modification to create derivatives with different structures and properties. So far three known derivatives of graphene have been successfully achieved in chemical reactions: graphene oxide (GO),<sup>15-18</sup> graphane (CH)<sup>19-22</sup> and recently fluorographene (CF).<sup>23-25</sup> Although GO is a wide band gap material that is important for device applications, its atomic structure, wherein the carbon atoms are decorated with epoxides, alcohols and carboxylic acid groups, is not suitable for nanoscale manipulations. CH obtained by exposing carbon honeycomb structure to hydrogen plasma, is another example of the graphene-based chemical derivative. Upon the hydrogenation, semimetallic graphene is converted into an insulator. CF, the two dimensional counterpart of teflon, is the most recent focus of graphene research.

Much recently, the fabrication of large graphene sheets having high-density array of nanoscale holes, called graphene nanomeshes (GNMs),<sup>26</sup> has been the landmark in controlling the electronic properties at nanoscale. Additionally, the formation of one-dimensional periodic Stone-Wales type defects producing metallic nanowires on graphene matrix has also been reported.<sup>27</sup> These recent advances have made mesh configuration a controllable parameters to monitor physical properties of nanostructures.<sup>26-28</sup> Earlier, interesting effects of periodically repeating holes in the electronic and mechanical properties of graphene nanoribbons were predicted from the first-principles calculations.<sup>29</sup>

In this paper, we apply supercell method to reveal the electronic, magnetic and mechanical properties of graphene which is patterned by various adsorbates or holes. The atomic structure of all adsorbates and holes are obtained after extensive structure optimiza-

tion. These periodically repeating superstructures or nanomeshes display properties which are rather different from those of graphene. We showed that not all patterns of adsorbates or hole with a 2D hexagonal lattice on graphene have linear band crossing, but only those which have a specific rotation symmetries. However, depending on the size of patterns or holes and the repeat periodicity, a GNM can be in different states ranging from to semiconducting including semimetallic with linear band crossing at the Fermi level.

## II. COMPUTATIONAL METHODOLOGY

The present study revealed crucial effects of the point group symmetry of nanomesh on the resulting properties. Here, we start with a brief discussion of hexagonal symmetry and apply simple tight binding model of  $\pi$ -orbitals to reveal the effect of lattice symmetry on the band crossing.<sup>30,31</sup> Graphene has the space group  $P6/mmm$  and point group symmetry  $D_{6h}$ . At the- $\Gamma$  point, the group of the wave vector is isomorphic to the point group  $D_{6h}$ .<sup>32</sup> However, irreducible representation of the wave vector point group turns into  $D_{2h}$  and  $D_{3h}$  at high symmetry points  $M$  and  $K$  (or  $K'$ ), respectively. It was shown that the tight binding Hamiltonian with nearest neighbor hopping parameter,  $t = 2.7$  eV

$$H = \sum_i \epsilon_i c_i^\dagger c_i + t \sum_{i,j} (c_i^\dagger c_j + H.c). \quad (1)$$

well approximates the  $\pi$ -bands of perfect graphene.<sup>30,31</sup> Here  $c_i^\dagger$  ( $c_i$ ) is the creation (annihilation) operator of a  $\pi$  electron at the lattice site  $i$ . The first term is the on-site energy of each carbon atom and equals to energy of the  $2p_z$  orbital. Energy eigenvalues of graphene and other two hypothetical crystal having square and hexagonal lattices with single atom in the cell are calculated and the contour plots their energy band gap in BZ are shown in Fig.1. For graphene, energy dispersion is linear at the vicinity of the  $K$ - symmetry (Dirac) points and the Fermi velocity, which is linearly dependent to nearest neighbor interaction parameter, can be given by the expression  $v_F = 3td/2\hbar$ .<sup>33</sup>

Hypothetical square lattice has semimetallic band structure as in Fig. 1(b). In the reciprocal space the band gap is closed along the boundaries of squares. However, differing from graphene, these bands do not have linear dispersion. The structure having hexagonal lattice with single  $\pi$ -orbital per unitcell is shown in Fig.1(c). Such a structure having a single  $\pi$ -orbital in each unitcell may also be realized by adatom saturation of one type (A- or B-type) carbon atoms of graphene. In this case, structure has three-fold rotation symmetry and hence six nearest neighbors. In this case, while saturation yields a dramatic change in the electronic structure, linear band crossings at Fermi level still occur at the points on a circle of radius  $R = \frac{4\pi}{3\sqrt{3}}$  in BZ. As shown in Fig. 1(c), this circle passes through the corners of hexagonal BZ of

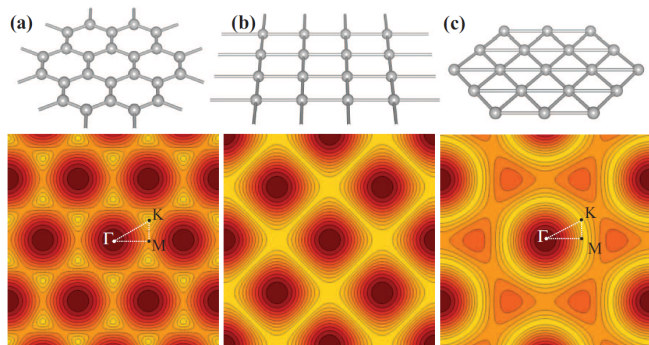


FIG. 1: Contour plots for band gap. (a) Perfect graphene. (b) A crystal having square lattice with single atom in the unit cell. (c) A crystal having hexagonal lattice with a single atom in the unit cell. Band crossing occurs along the yellow/light contours on which the band gap becomes zero. Band gap takes its maximum value at brown/dark contours.

graphene. The Fermi velocity is calculated to be in the order of  $10^6$  m/s in the vicinity of band crossing points.

While the tight binding model allowed us to understand the general features of the band gap in different lattices, it fails to account for the reconstruction and re-bonding near the defect. In the rest of the paper we perform calculations from the first-principles to investigate various types of defects. To this end we carried out spin-polarized plane wave calculations<sup>34,35</sup> using local density approximation (LDA)<sup>36</sup> and projector augmented wave (PAW)<sup>37</sup> potential. Patterns of defects are treated using supercell geometry, where a minimum of  $10 \text{ \AA}$  vacuum spacing is kept between the adjacent graphene layers. Kinetic energy cutoff, Brillouin zone (BZ) sampling are determined after extensive convergence analysis. For the plane-wave basis set, the kinetic energy cutoff is taken to be  $\hbar^2|\mathbf{k} + \mathbf{G}|^2/2m = 500$  eV. For partial occupancies Methfessel-Paxton smearing method<sup>38</sup> is used. The convergence criterion of self-consistent field calculations is  $10^{-5}$  eV for total energy values. By using the conjugate gradient method, all atomic positions and the size of unitcell were optimized until the atomic forces were less than  $0.05$  eV/ $\text{\AA}$ . Pressures on the lattice unit cell are decreased to values less than  $1$  kB.

## III. ADATOM PATTERNED GRAPHENE NANOMESHES

In this section we show how a periodic decoration of graphene by adatoms modifies the electronic structure. Here we considered H, F, O and Mn adatoms, which are adsorbed at different sites and form a  $(4 \times 4)$  supercells on graphene host matrix as shown in Fig.2(a)-(d). We did not consider the interstitial or substitutional decoration, since experimental studies treating various foreign atoms, such as N<sup>8</sup>, O<sup>15</sup>, H<sup>19</sup>, F<sup>23</sup>, C<sup>39</sup>, Co<sup>40</sup>, Fe and Gd<sup>41</sup>, Au and Pt<sup>42</sup>, revealed that these atoms prefer to be adsorbed at various sites on the surface of graphene,

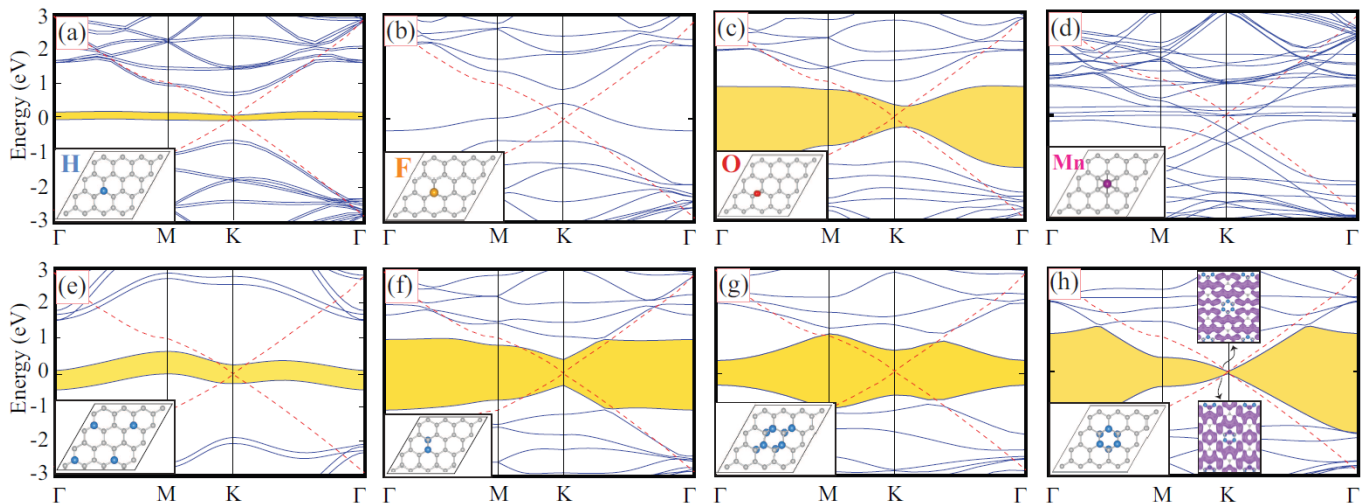


FIG. 2: Spin-polarized energy band structure of a periodic patterns consisting of the (4x4) supercells each having a single (a) hydrogen; (b) fluorine; (c) oxygen; (d) manganese adatom. (e) A similar hydrogen pattern forming the (2x2) supercell on graphene host matrix allowing significant coupling between adatoms. (f-h) Periodic patterns of two, eight and six hydrogen atoms in the (4x4) graphene supercell, respectively. Isosurface of charge density of bands crossing near the  $K$ -point are shown by insets. For the sake of comparison, linearly crossing  $\pi$  and  $\pi^*$ -bands of perfect graphene host matrix are also superimposed in the band structures. The zero of energy is set at the Fermi level  $E_F$ . The band gaps are shaded in yellow. All the bands presented in BZ corresponding to the (4x4) supercell.

but none of them is adsorbed at the interstitial sites, nor is substituted for carbon atom.

Owing to the unpaired electron, a single hydrogen adatom adsorbed to the (4x4) supercell has a spin polarized, semiconducting ground state with a net magnetic moment of  $\mu=1 \mu_B$ . Upon the adsorption of a hydrogen atom band structure of graphene changes dramatically. Instead of linear crossing of  $\pi$  and  $\pi^*$ -bands at Fermi level, dispersionless impurity bands occurs with 0.1 eV indirect band gap. Similar to hydrogen atom, the most favorable adsorption site for a F atom on graphene is the top site of carbon atoms. Upon the adsorption of a F atom,  $sp^2$  bondings of three C-C bonds below F atom are dehybridized and form tetrahedrally coordinated four  $sp^3$  type bondings. Differing from the decoration of H adatom, ground state is nonmagnetic and as a result of odd number of electrons F decorated graphene becomes metalized as shown in Fig. 2(b). The band crossing at the  $K$ -points does not occur, since F adsorbed at the top of C atom changes the sixfold rotation symmetry to the threefold rotation symmetry.

Oxygen atom favors the bridge site between two underlying C atoms. Upon the adsorption of an oxygen at the bridge site two underlying C atoms become buckled by 0.36 Å. C-C and C-O bonds are calculated to be 1.51 and 1.44 Å, respectively. Resulting structure is a nonmagnetic semiconductor with 0.63 eV direct band gap (Fig. 2(c)). Valence and conduction band edges occurs between the  $K$ - and  $\Gamma$ -points. The adatom at the bridge site breaks the six fold rotation symmetry and hence hinders the linear band crossing.

The situation is different in the case of Mn, which is

adsorbed above the center of a hexagon in graphene matrix and induces negligible deformation. Only six nearest C atoms raise slightly to higher (0.02 Å) position relative to the plane. Localized, non-bonding Mn-3d orbitals form flat bands near the Fermi level. On the other hand, the sixfold rotation symmetry is maintained even after Mn atom adsorbed at the hollow site above the center of hexagon. Accordingly, the metallic structure with a net magnetic moment of  $3 \mu_B$  per cell allows linear crossing of graphene bands at the  $K$ -points in Fig. 2(d).

Having discussed the effect of periodic decoration by single adatoms, we next consider the periodic patterns of adatom groups. In Fig. 2(e) we show electronic band structure corresponding to relatively denser hydrogen coverage (C:H=8). Such a nanomesh created by one-sided decoration of four hydrogen atoms in the (4x4) supercell gives rise to a relatively dispersive bands and a net magnetic moment of  $4 \mu_B$  per supercell. Since the six fold rotation symmetry of graphene is broken by adsorbed H atoms, linear crossing of bands do not occur. In a decoration involving two sides of graphene, where two adjacent C atoms of different sublattices are saturated from different sides as shown in Fig. 2 (f). Since an equal number of A- and B-sublattice atoms are saturated, the structure is nonmagnetic semiconductor with a band gap of 0.8 eV. Another pattern derived from a graphene like domain consisting of 8 H atoms in Fig. 2(g) results in a band gap of 0.7 eV at  $\Gamma$ -point, but larger gap of 1 eV at the  $K$ -point. This nanomesh presents an electronic structure rather different both from graphene and graphane. The electronic structure is, however, different for a pattern of six H atoms, which saturate six carbon atoms at

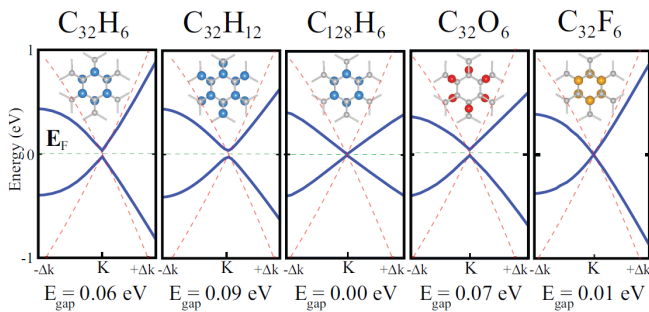


FIG. 3: Band structures showing the effects of the coupling between various patterns as a function of their size and the size of mesh (supercell). The linearly crossing of  $\pi$ - and  $\pi^*$ -bands of graphene are shown by red/dashed lines.

the corner a hexagon alternatingly from different sites; namely three of them adsorbed to A-sublattice from one side, remaining three adsorbed to B-sublattice from the other side. Even though sixfold rotation symmetry has changed to  $S_6$  symmetry, both point group symmetries allow linear band crossing as seen in Fig. 2(h). This case demonstrates the crucial role played by the intrinsic symmetry of the pattern in determining the electronic structure.<sup>11–13</sup>

Let us now take a closer look at the triangular patterns of adatom groups that have hexagonal symmetry. In Fig. 3, we plot these  $\pi$ - and  $\pi^*$ -bands in the vicinity ( $\Delta k=0.03 \text{ \AA}^{-1}$ ) of  $K$ -symmetry point for different patterns on supercells of different sizes; namely the (4x4) and (8x8) ( $C_{128}$  and  $C_{32}$ ) supercells.  $H_6$  and  $H_{12}$  patterns which have 0.06 and 0.09 eV band gap at  $K$ -point, indicates that the band gap opening increases with increasing pattern size and hence increasing coupling. In the (8x8) supercell the interaction between periodically repeating  $H_6$  patterns is hindered and hence linear crossing of  $\pi$ - and  $\pi^*$ -bands at  $K$ -symmetry point similar to bare graphene is attained. By expressing these bands as  $\mathbf{k} = \mathbf{K} + \mathbf{q}$  and by neglecting the second order terms with respect to  $q^2$ , the dispersion of the energy bands can be given as  $E(\mathbf{q}) \simeq \mathbf{v}_F \hbar |\mathbf{q}|$ . Here the Fermi velocity  $v_F$  is calculated as  $0.7 \times 10^6 \text{ m/s}$  (i.e.  $\sim 0.6$  of the Fermi velocity calculated for Dirac Fermions in perfect graphene).

We also present an example of  $O_6$  pattern analogous to  $H_{12}$  decoration of (4x4) supercell ( $C_{32}H_{12}$ ) of graphene in Fig. 3. In this pattern three O atoms are bound alternatingly to bridge site at one site, the remaining three to other site. Here it is seen that denser O patterns are not favored due to strong O-O repulsion. Linear crossing of bands at  $K$ -point can also be achieved by O adatoms forming a periodically repeating  $O_6$  pattern. Small band gap in Fig. 3 can be closed if the supercell size is increased to hinder coupling between them. This example implies that the patterns similar to that done by using H atoms can be created by the passivation of  $p$ -orbital electrons with O atoms. In the case of fluorination of (4x4) graphene by  $F_6$  decoration, similar to  $H_6$ , linear  $\pi$

and  $\pi^*$ -bands gets closer with very small (0.01 eV) band gap at  $K$ -point. Finally, the isosurface charge densities of these linearly crossing bands near  $K$ -point indicates that they mainly originate from graphene  $\pi$ -orbitals with small mixing from the adatom (see Fig. 2 (h)).

#### IV. HOLE PATTERNED GRAPHENE NANOMESHES

Similar to adatom patterns on graphene, nanomeshes generated from the holes periodically patterned on graphene matrix exhibit also interesting features. This conclusion drawn from theoretical calculations are in line with the findings obtained from the fabrication of GNMs by means of block-copolymer assisted nanopatterning process. It has been shown that GNMs having high-density periodic array of holes display promising advantages relative to existing graphene devices.<sup>26,27</sup> Thanks to the advances in the preparation of high quality nanoscale hard masks<sup>26,27,43</sup> in laboratory conditions, theoretical studies in this field become more relevant for applications. Here we carry out calculations for the holes having 1-2 nm repeat period and 2-10  $\text{\AA}$  diameter. In Fig. 4(a) we describe the geometric parameters of  $C_n$  hole defects forming a hexagonal lattice, where  $n$  denotes number of C atoms removed from graphene matrix to make a hole. For nanoholes, we define the hole size as the maximum diameter of the  $C_n$  hole defected region. After the creation of a  $C_1$  defect (i.e. single C vacancy), Jahn-Teller type distortion changes the positions of surrounding C atoms slightly. The resulting structure attains a net magnetic moment of  $1 \mu_B$ . The origin of magnetism in defected graphene sheets and the character of electronic states induced by the vacancy resulting in flat bands around Fermi level have been investigated by some recent studies.<sup>44–46</sup> Upon the removal of C atoms ( $n>1$ ) graphene is reconstructed to result in a significant modification in atomic configuration around the hole. For example, after the relaxation of atomic structure,  $C_2$  defected region becomes an octagon-shaped hole surrounded by 2 pentagons and 6 hexagons. Similarly, as a result of Stone-Wales type transformation, each  $C_4$  defect region also turns into a nonagon-shaped hole. As it was reported experimentally,<sup>47</sup> a hole region is surrounded by pentagonal and hexagonal rings of C atoms to keep the flatness of the sheet. While the honeycomb lattice symmetry of the graphene matrix does not change considerably for larger defects  $C_6$  and  $C_{24}$ , hole region of  $C_{12}$  takes almost a circular shape surrounded by regular pentagons and hexagons. Apparently, the trend in the shape of the hole region is determined by whether the edges of domain are zigzag or armchair shaped.

The energy band structures of graphene nanomeshes exhibit interesting variations with respect to their sizes, diameters and shapes of nanohole as illustrated in Fig.4 (b). While nanomesh of  $C_1$  defect have metallic behavior, periodic structure of  $C_2$  defect becomes indirect band



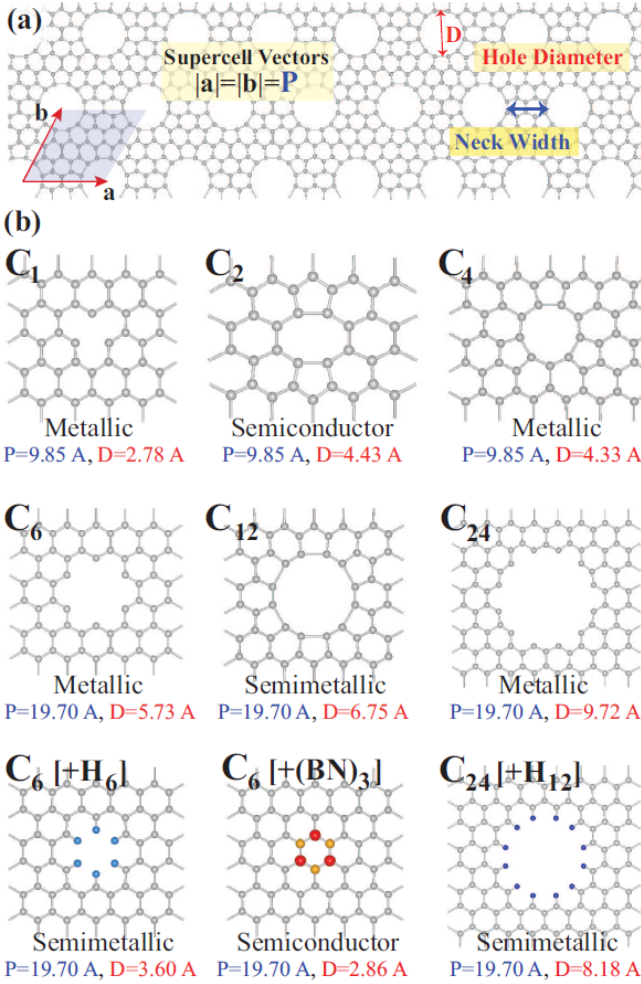


FIG. 4: (a) Structural parameters for a nanomesh of  $C_n$  hole. (b) Large supercells of hexagonal lattice each containing single hole of  $C_1$ ,  $C_2$ ,  $C_4$ ,  $C_6$ ,  $C_{12}$ ,  $C_{24}$ . The nanomeshes in the third row are obtained by saturating  $C_6$  and  $C_{24}$  holes by hydrogen and also by B and N atoms alternately.

gap semiconductor of 0.65 eV. However,  $\pi$  and  $\pi^*$ -bands above the Fermi level still very close to each other (0.09 eV gap) at the  $K$ -point.  $C_4$  defected GNM has metallic behavior. The situation becomes even more remarkable for larger defects  $C_6$ ,  $C_{12}$  and  $C_{24}$ . GNMs including either  $C_6$  or  $C_{24}$  hole have zigzag edges and are metals with antiferromagnetic (AFM) ground state. We note that the defect induced flat electronic bands around the Fermi level occur if the electron spins become unpaired. On the other hand, the reconstruction or the dimerization of carbon dangling bonds around the defect can cause the flat bands in the gap to disappear. Interestingly, nanomeshes of  $C_6$  and  $C_{24}$  holes, which are metallic, become semimetal upon the saturation of dangling bonds of carbon atoms around the hole by hydrogen atoms. This metal-semimetal transformation can have applications in graphene-based nanoelectronics. On the other hand, GNM of  $C_6$  turns semiconducting with a band gap

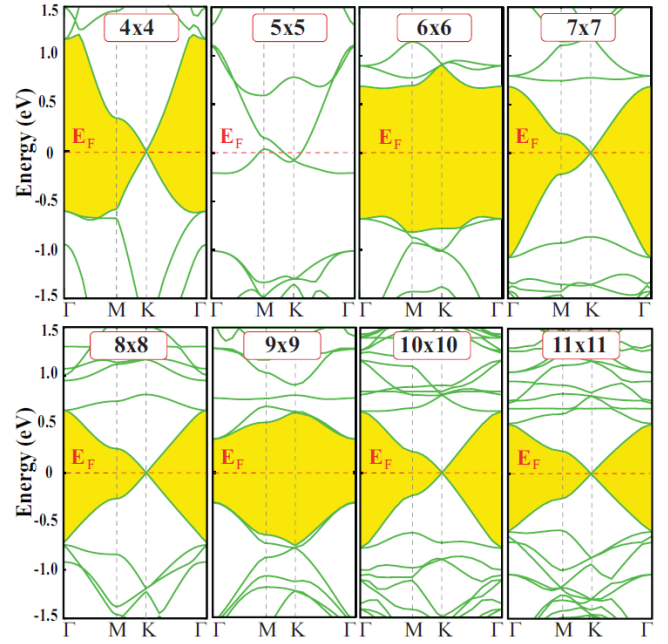


FIG. 5: Band structure of nanomeshes of  $C_{12}$  forming in the  $(n \times n)$  supercells of graphene with  $n=4 \dots 11$ .

of 0.1 eV upon the termination of the dangling bonds of C atoms around the hole by B and N alternatingly to form a  $B_3N_3$  hexagon. The band opening is explained by the breaking of sixfold symmetry due to  $B_3N_3$  hexagon. The formation extended  $B_nN_n$  honeycomb structure can be achieved directly in the course of epitaxial growth of graphene and single layer BN.<sup>48,49</sup>

As for GNM with  $C_{12}$ , it is a nonmagnetic semimetal because of carbon atoms at the edge are dimerized. The analysis of the orbital character of linearly crossing  $\pi$ - and  $\pi^*$ -bands near  $K$ -point using isosurface charge densities suggests that these bands originate from bonding and antibonding combinations of  $\pi$ -orbitals at the neck and around  $C_6$  hole. Here we discuss an important aspect of GNMs with  $C_{12}$ , that the size of the hexagonal supercell or repeat periodicity of  $C_{12}$  is crucial for the resulting electronic structure. Fig. 5 shows band structures of GNMs including single  $C_{12}$  hole in the supercell of  $(n \times n)$  where  $n=4 \dots 11$ . For  $n=4$ , GNM has the neck region consisting of single hexagon is a semimetal. For  $n=5$ , GNM is a metal and has a neck region which is relatively thicker, but its C-C bond angles strongly deviate from  $120^\circ$ . Surprisingly, GNM with  $n=6$  is a semiconductor having 1.3 eV band gap. The bond angles still continue to deviate from those of graphene. However, from  $n=7$  on the bond angles at the neck region start to be graphene like with regular honeycomb structure. Both GNMs with  $n=7$  and 8 are semimetals and have  $\pi$ - and  $\pi^*$ -bands which linearly cross at Fermi level at the  $K$ -point. Isosurface charge densities of these bands near  $K$ -points demonstrate that they, in fact, originate from the combination of graphene  $\pi$ -orbitals. As  $n$  increases,

GNM exhibit the similar trend for  $n=6-9$ ; namely it is semiconductor for  $n=9$ , but semimetals for  $n=10$  and  $11$ . This variation of band gaps is reminiscent of the family behavior of graphene nanoribbons and is related to the variation of the thickness of necks between periodically repeating  $C_{12}$  holes.<sup>29,50</sup> Here, even if the six fold rotation symmetry is conserved, the band gap opens for every  $n=3 \times N$  with  $N$  being an integer  $\geq 2$ . However, this gap becomes smaller and eventually is closed as  $n \rightarrow \infty$ . We also note that the family like behavior of GNMs is related with the edge structure of the hole. In regard to the size of GNM of  $C_{12}$ , we note also that the lattice constants of corresponding  $(n \times n)$  supercell is modified with size. For example, for  $n=11$ , the lattice constant of supercell is contracted by 1%, the contraction is 4% for  $n=5$  and 40% for  $n=4$ .

Finally, in addition to triangular defect patterns, we also discuss the electronic structure of holes arranged in a rectangular lattice. In Fig. 6 we show the electronic band structures of  $C_{12}$  nanomeshes realized by the supercells of  $(3 \times 6)$ ,  $(4 \times 8)$  and  $(5 \times 10)$ . While  $C_{12}$  holes in a small rectangular supercells with small repeat periodicity (leading to significant coupling) become semiconducting, the semimetallic nature indigenous to graphene is achieved in large supercells. As shown in Fig. 6(c), even if the rotation symmetry required for band crossing is absent, graphene-like Bloch wave functions in the rectangular mesh of sparse patterns of  $C_{12}$  holes show a semimetallic behavior. This indicates that as the size of the supercell becomes larger and the neck gets wider relative to the size of the hole, the symmetry requirement necessary for the linear band crossing can be relaxed.

## V. MECHANICAL PROPERTIES OF NANOMESHES

Honeycomb structure with  $sp^2$  bonding underlies the unusual mechanical properties providing very high in-plane strength, but transversal flexibility. Here we investigate how the mechanical properties of nanomeshes generated with patterns of adatoms or holes. We focused on the harmonic range of the elastic deformation, where the structure responded to strain  $\epsilon$  linearly. Here  $\epsilon$  the elongation per unit length. The strain energy is defined as  $E_s = E_T(\epsilon) - E_T(\epsilon = 0)$ ; namely, the total energy at a given strain  $\epsilon$  minus the total energy at zero strain. Normally, the Young's modulus is the value, which characterizes the mechanical strength of a bulk material. Owing to ambiguities in defining the Young's modulus of two dimensional structures like a GNM, one can use in-plane stiffness  $C = (1/A_0) \cdot (\partial^2 E_s / \partial \epsilon^2)$  in terms of the equilibrium area of the supercell,  $A_0$ .<sup>51,52</sup> We calculated the in-plane stiffness of graphene, and nanomeshes consisting of  $C_{32}H_6$ , BN substituted graphene (i.e  $C_{26}[(BN)_3]$  and  $C_6$  hole in graphene using  $(4 \times 4)$  supercell in Fig. 3. The stiffness of bare graphene is calculated to be 334 N/m, which is in good agreement with the experimental value

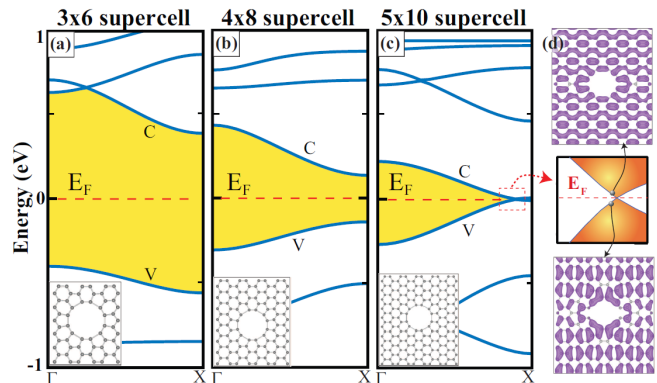


FIG. 6: (a)-(c) Rectangular patterns of  $C_{12}$  holes repeated in  $(3 \times 6)$ ,  $(4 \times 8)$  and  $(5 \times 10)$  graphene supercells. Atomic structure of nanomeshes are given by inset. (d) Semimetallic electronic structure and isosurface charge densities of valence (V) and conduction (C) bands of  $(5 \times 10)$  nanomesh are also shown.

of  $340 \pm 50$  N/m. Furthermore, the in-plane stiffness values of nanomeshes generated on graphene through  $B_3N_3$  substitution,  $H_6$  adatom pattern and  $C_6$  hole are 308 N/m, 283 N/m and 167 N/m, respectively. Apparently, the bare graphene matrix is weakened by the formation of any of these nanomeshes. In addition to the calculation of in-plane stiffness, we extend our analysis to include the plastic deformation region, where the honeycomb like structure is destroyed after the yielding point (i.e. on set of plastic deformation), and GNM undergoes a massive structural deformation. Our preliminary simulations indicate that the yielding strain of  $C_6$  hole GNM is significantly lower than the yielding strains of both  $C_{26}[(BN)_3]$  and  $C_{32}H_6$  GNMs.

## VI. CONCLUSIONS

While graphene and its various derivatives, GO, CH and CF, are important nanomaterials with diverse electronic, magnetic and mechanical properties, their properties can be modified and multiplied using different methods of functionalization. The most pronouncing property of graphene, namely linearly crossing bands at the Fermi level and electron-hole symmetry arising therefrom is usually destroyed, when graphene is functionalized through dopant or vacancy defects. In this work we demonstrated that the electron-hole symmetry, even Dirac Fermion behavior can be recovered for periodically repeating superstructures or nanomeshes having special point group symmetry. In this study we considered nanomeshes, which are generated by the decoration of adatoms, adatom groups or holes, which repeats periodically in graphene matrix. We found that types of adatoms and their patterns, the geometry of the holes of carbon atoms, the sizes and lattice symmetries of nanomesh provide us with several parameters to engineer the electronic and magnetic properties of the

nanomesh. In particular, we showed that by varying only the size of the nanomesh including a specific hole one can tune between metallic and semiconducting state including semimetal with linearly crossing bands. This is reminiscent of the family behavior of graphene nanoribbons.

## VII. ACKNOWLEDGMENTS

This work is supported by TUBITAK through Grant No:108T234. Part of the computational resources has

been provided by TUBITAK ULAKBIM, High Performance and Grid Computing Center (TR-Grid e-Infrastructure). We also thank the DEISA Consortium (www.deisa.eu), funded through the EU FP7 project RI-222919, for support within the DEISA Extreme Computing Initiative. S. C. acknowledges the partial support of TUBA, Academy of Science of Turkey.

- 
- \* Electronic address: ciraci@fen.bilkent.edu.tr
- <sup>1</sup> A. K. Geim, K. S. Novoselov, *Nat. Mater.* **6**, 183 (2007).
  - <sup>2</sup> X. Wang, Y. Ouyang, X. Li, H. Wang, J. Guo, H. Dai, *Phys. Rev. Lett.* **100**, 206803 (2008).
  - <sup>3</sup> C. Berger, Z. Song, T. Li, X. Li, A. Y. Ogbazghi, R. Feng, Z. Dai, A. N. Marchenkov, E. H. Conrad, P. N. First, and W. A. de Heer, *Science* **312**, 1191 (2006).
  - <sup>4</sup> Y. Zhang, Yan-Wen Tan, H. L. Stormer, and P. Kim, *Nature (London)* **438**, 201 (2005).
  - <sup>5</sup> S. Cahangirov, M. Topsakal, E. Akturk, H. Şahin and S. Ciraci, *Phys. Rev. Lett.* **102**, 236804 (2009).
  - <sup>6</sup> H. Şahin, S. Cahangirov, M. Topsakal, E. Bekaroglu, E. Aktürk, R. T. Senger, and S. Ciraci, *Phys. Rev. B* **80**, 155453 (2009).
  - <sup>7</sup> J. M. Garcia-Lastra, *Phys. Rev. B* **82**, 235418 (2010).
  - <sup>8</sup> L. S. Panchakarla, K. S. Subrahmanyam, S. K. Saha, A. Govindaraj, H. R. Krishnamurthy, U. V. Waghmare, and C. N. R. Rao, *Adv. Mater.* **21**, 4726 (2009).
  - <sup>9</sup> H. Şahin and R. T. Senger, *Phys. Rev. B* **78**, 205423 (2008).
  - <sup>10</sup> H. Şahin, R. T. Senger and S. Ciraci, *J. Appl. Phys.* **108**, 074301 (2010)
  - <sup>11</sup> R. Martinazzo, S. Casolo, and G. F. Tantardini, *Phys. Rev. B* **81**, 245420 (2010).
  - <sup>12</sup> R. P. Tiwari and D. Stroud, *Phys. Rev. B* **79**, 205435 (2009).
  - <sup>13</sup> C. -H. Park and S. G. Louie, *Nano Lett.* **9**, 1793 (2009).
  - <sup>14</sup> M. Gibertini, A. Singha, V. Pellegrini, M. Polini, G. Vignale, A. Pinczuk, L. N. Pfeiffer, and K. W. West, *Phys. Rev. B* **79**, 241406 (2009).
  - <sup>15</sup> D. A. Dikin, S. Stankovich, E. J. Zimney, R. D. Piner, G. H. B. Dommett, G. Evmenenko, S. T. Nguyen, and R. S. Ruoff, *Nature (London)* **448**, 457 (2007).
  - <sup>16</sup> S. Stankovich, R. D. Piner, X. Chen, N. Wu, S. T. Nguyen, R. S. Ruoff, *J. Mater. Chem.* **16**, 155 (2006).
  - <sup>17</sup> G. Eda, G. Fanchini and M. Chhowalla, *Nature Nanotech.* **3**, 270 (2008).
  - <sup>18</sup> C. Gomez-Navarro, R. T. Weitz, A. M. Bittner, M. Scolari, A. Mews, M. Burghard, and K. Kern, *Nano Lett.* **7**, 3499 (2007).
  - <sup>19</sup> D. C. Elias, R. R. Nair, T. M. G. Mohiuddin, S. V. Morozov, P. Blake, M. P. Halsall, A. C. Ferrari, D. W. Boukhvalov, M. I. Katsnelson, A. K. Geim, and K. S. Novoselov, *Science* **323**, 610 (2009).
  - <sup>20</sup> J. O. Sofo, A. S. Chaudhari and G. D. Barber, *Phys. Rev. B* **75**, 153401 (2007).
  - <sup>21</sup> H. Şahin, C. Ataca, and S. Ciraci, *Appl. Phys. Lett.* **95**, 222510 (2009).
  - <sup>22</sup> M. Z. S. Flores, P. A. S. Autreto, S. B. Legoas and D. S. Galvao, *Nanotechnology* **20**, 465704 (2009).
  - <sup>23</sup> R. R. Nair, W. Ren, R. Jalil, I. Riaz, V. G. Kravets, L. Britnell, P. Blake, F. Schedin, A. S. Mayorov, S. Yuan, M. I. Katsnelson, H.-M. Cheng, W. Strupinski, L. G. Bulusheva, A. V. Okotrub, I. V. Grigorieva, A. N. Grigorenko, K. S. Novoselov, and A. K. Geim, *Small* **6**, 2877 (2010).
  - <sup>24</sup> S. -H. Cheng, K. Zou, F. Okino, H. R. Gutierrez, A. Gupta, N. Shen, P. C. Eklund, J. O. Sofo, and J. Zhu, *Phys. Rev. B* **81**, 205435 (2010).
  - <sup>25</sup> H. Şahin, M. Topsakal and S. Ciraci, *Phys. Rev. B* **83**, 115432 (2011).
  - <sup>26</sup> J. Bai, X. Zhong, S. Jiang, Y. Huang and X. Duan, *Nature Nanotech.* **5**, 190 (2010).
  - <sup>27</sup> J. Lahiri, Y. Lin, P. Bozkurt, I. I. Oleynik, and M. Batzill, *Nature Nanotech.* **5**, 326 (2010).
  - <sup>28</sup> R. Balog, B. Jorgensen, L. Nilsson, M. Andersen, E. Rienks, M. Bianchi, M. Fanetti, E. Lagsgaard, A. Baraldi, S. Lizzit et al., *Nat. Mater.* **9**, 315 (2010).
  - <sup>29</sup> M. Topsakal, E. Akturk, H. Sevincli and S. Ciraci, *Phys. Rev. B* **78**, 235435 (2008).
  - <sup>30</sup> P. R. Wallace, *Phys. Rev.* **71** 622 (1947).
  - <sup>31</sup> C. Bena and G. Montambaux, *New J. Phys.* **11** 095003 (2009).
  - <sup>32</sup> L. M. Malard, M. A. Pimenta, G. Dresselhaus and M. S. Dresselhaus, *Physics Reports* **473**, 51 (2009).
  - <sup>33</sup> A. H. Castro Neto, F. Guinea, N. M. R. Peres, K. S. Novoselov, and A. K. Geim, *Rev. Mod. Phys.* **81**, 109 (2009).
  - <sup>34</sup> G. Kresse, J. Hafner, *Phys. Rev. B* **47**, 558 (1993).
  - <sup>35</sup> G. Kresse, J. Furthmüller, *Phys. Rev. B* **54**, 11169(1996).
  - <sup>36</sup> D. M. Ceperley and B. J. Alder, *Phys. Rev. Lett.* **45**, 566 (1980).
  - <sup>37</sup> P. E. Blochl, *Phys. Rev. B* **50**, 17953 (1994).
  - <sup>38</sup> M. Methfessel and A. T. Paxton, *Phys. Rev. B* **40**, 3616 (1989).
  - <sup>39</sup> A. Hashimoto, K. Suenaga, A. Gloter, K. Urita and S. Iijima, *Nature* **430**, 870 (2004).
  - <sup>40</sup> V. W. Brar, R. Decker, Hans-Michael Solowan, Y. Wang, L. Maserati, K. T. Chan, H. Lee, C. O. Girit, A. Zettl, S. G. Louie, M. L. Cohen and M. F. Crommie, *Nature Physics* **7**, 43 (2011).
  - <sup>41</sup> M. Hupalo, S. Binz and M. C. Tringides, *J. Phys.: Condens. Matter* **23** 045005 (2011).

- <sup>42</sup> Y. Gan, L. Sun, and F. Banhart, *Small* **4**, 587 (2008).
- <sup>43</sup> L. Zhang, S. Diao, Y. Nie, K. Yan, N. Liu, B. Dai, Q. Xie, A. Reina, J. Kong and Z. Liu, *J. Am. Chem. Soc.*, to be published.
- <sup>44</sup> E. H. Lieb, *Phys. Rev. Lett.* **62**, 1201 (1989).
- <sup>45</sup> O. V. Yazyev and L. Helm, *Phys. Rev. B* **75**, 125408 (2007).
- <sup>46</sup> B. R. K. Nanda, M. Sherafati, Z. Popovic and S. Satpathy, arXiv:1105.1129
- <sup>47</sup> A. Hashimoto, K. Suenaga, A. Gloter, K. Urita, and S. Iijima, *Nature (London)* **430**, 870 (2004).
- <sup>48</sup> S. Cahangirov and S. Ciraci, *Phys. Rev. B* **83**, 165448 (2011).
- <sup>49</sup> L. Ci, L. Song, C. Jin, D. Jariwala, D. Wu, Y. Li, A. Srivastava, Z. F. Wang, K. Storr, L. Balicas, F. Liu, and P. M. Ajayan, *Nat. Mater.* **9**, 430 (2010).
- <sup>50</sup> S. Cahangirov, M. Topsakal, and S. Ciraci, *Phys. Rev. B* **81**, 195120 (2010).
- <sup>51</sup> B. I. Yakobson, C. J. Brabec, J. Bernholc, *Phys. Rev. Lett.* **76**, 2511 (1996).
- <sup>52</sup> C. D. Reddy, S. Rajendran, K. M. Liew, *Nanotechnology* **17** 864 (2006).